Available online at www.sciencedirect.com
SCIENCE DIRECT®
Catalysis Today 90 (2004) 77–83
CATALYSIS TODAY
www.elsevier.com/locate/cattod

Direct decomposition of NO in a monolith reactor: comparison of mathematical models

Vesna Tomašić*, Stanka Zrnčević, Zoran Gomzi

Faculty of Chemical Engineering and Technology, University of Zagreb, Zagreb, Croatia

Abstract

This work describes the research aimed at developing mathematical model for predicting the performance of the monolith reactor. Two heterogeneous models were applied to describe a single channel of the reactor. Comparison between the mass transfer coefficients, obtained using the model with 1D description of the gas phase and 2D description of the solid phase and a complete 2D model (2D description of both gas and solid phase) was made and discussed. The proposed models were verified by comparing the experimental data with theoretical predictions. Particular emphasis was put on the interphase mass transfer.

Keywords: Mass transfer; Mathematical modelling; Monolith reactor; Washcoat; Zeolite Cu/ZSM-5

1. Introduction

The monolithic reactors are widely used to reduce the emissions of undesired products and combustion by-products. Their advantages over the conventional multi-phase reactors (slurry and packed-bed reactors) expanded their applications, e.g. in cleaning of automotive exhaust gases, selective catalytic reduction of nitrogen oxides, catalytic abatement of volatile organic compounds from industrial processes, catalytic fuel combustion, stream reforming of hydrocarbons, etc. [1–5].

In general, a monolithic reactor consists of the thin parallel straight channels of arbitrary shape, through which a gas, containing the reactants, flows. The walls of the channels are usually coated with a porous ceramic containing the catalyst layer (or washcoat). Conversion from the reactants to products involves the transport by convective flow through the channels and molecular diffusion towards the channel walls. Simultaneous diffusion and chemical reaction occur inside the porous washcoat, whereby the products diffuse back into the gas and are transported from the reactor [6].

Customary analysis of a monolith reactor is based on one-dimensional (1D) model where the complexities of the radial interphase transport are lumped into the gas–solid mass transfer coefficient [7]. This approach usually invokes analogy with the Greatz–Nusselt problem governing heat transfer into fluid under the laminar flow in a duct at constant wall temperature. A detailed description of the monolith reactor can be obtained by means of multi-dimensional models. Multi-dimensional modelling enables formal calculation of the local mass transfer coefficients along the monolith, relevant to hydrodynamic regime in the monolith reactor. This approach allows a reasonably accurate prediction of the monolith performance under diffusion-limited conditions.

This study is the continuation of our previous investigation of the performances of the monolith reactors during NO decomposition [8,9]. In this work two different heterogeneous models of the monolith reactor were used and analysed, with the aim of determining the importance of mass transfer effects and resolving the issue of the correct values of local Sherwood numbers and corresponding mass transfer coefficients inside the monolith reactor.

2. Experimental

2.1. Catalyst preparation and characterisation

Zeolite-based monoliths (Cu/ZSM-5 on cordierite) were prepared using the “washcoat” method [10,11]. Starting materials for preparation of the monoliths were ceramic

* Corresponding author. Tel.: +385-1-4597103; fax: +385-1-4597133.
E-mail address: vtomas@fkit.hr (V. Tomašić).

0920-5861/$ – see front matter © 2004 Elsevier B.V. All rights reserved.
doi:10.1016/j.cattod.2004.04.011

Nomenclature

a	geometric surface area of the channel (m^2)
C_{A_0}	initial concentration of NO ($mol\,m^{-3}$)
$C_{A,f}$	concentration in the fluid phase ($mol\,m^{-3}$)
$\bar{C}_{A,f}$	average concentration in the fluid phase ($mol\,m^{-3}$)
$C_{A,s}$	concentration in the solid phase ($mol\,m^{-3}$)
C_{NO^*}	concentration of adsorbed NO ($mol\,m^{-3}$)
C_{O^*}	concentration of adsorbed O ($mol\,m^{-3}$)
C_{O_2}	concentration of oxygen ($mol\,m^{-3}$)
C_t	total concentration of active sites ($mol\,m^{-3}$)
C_*	concentration of vacant sites ($mol\,m^{-3}$)
d_{ch}	equivalent diameter of the monolith channel (m)
D_e	effective diffusion coefficient in the washcoat ($m^2\,s^{-1}$)
D_f	molecular diffusion coefficient ($m^2\,s^{-1}$)
k	rate constant (Eq. (13)) ($m^3\,mol^{-1}\,s^{-1}$)
k_m	mass transfer coefficient ($m\,s^{-1}$)
k_S	surface reaction rate constant (Eq. (18)) ($m^3\,mol^{-1}\,s^{-1}$)
K_A	adsorption equilibrium constant for NO ($m^3\,mol^{-1}$)
K'_D	adsorption equilibrium constant for oxygen ($m^3\,mol^{-1}$)
r	radial coordinate (m)
$r_{A,s}$	surface reaction rate ($mol\,m^3\,s^{-1}$)
r_{ch}	equivalent radius of the monolith channel (m)
R	overall radius ($r_{ch} + \delta_e$) (m)
Sh	local Sherwood number (–)
T	temperature (K)
u	linear velocity of gas phase ($m\,s^{-1}$)
y_i	molar fraction of compound i (–)
z	axial coordinate (m)
Z	length of the monolith (m)

Greek symbol

δ_e	equivalent thickness of the washcoat (m)

honeycomb substrate (cordierite) and copper containing ZSM-5 zeolite, Cu/ZSM-5 (Si/Al = 40; 1.92 wt.% Cu). Main properties of the cordierite honeycomb substrate were: squarely structured channels; 31 channels cm^{-2}, channel spacing—1.803 mm; wall thickness—0.267 mm and hydraulic diameter—1.537 mm. The commercial oval type of honeycomb was cut into square pieces, each with four channels. The samples 75 mm long were used for coating of the catalytic layer. Copper ions were incorporated into the zeolite by ion exchange of Na/ZSM-5 in the aqueous solution of cupric acetate. Copper ion exchange step had been performed before coating the monolith.

To washcoat the monolith, a slurry was prepared by suspending Cu/ZSM-5 zeolite in the aqueous solution of aluminium nitrate. Two monolith catalysts, labelled MZ1 and MZ2, were prepared with catalytic washcoat of different thickness. A detailed description of the monolith catalyst preparation can be found elsewhere [8].

The prepared monolith samples were characterised by several techniques, such as XRD, SEM, surface measurements and mercury porosimetry. Textural properties, such as specific surface area, total pore volume and mean pore radius are given in [9].

2.2. Experimental apparatus and procedures

Before the reaction, the monolith catalyst had been treated in situ at 773 K for 2 h under helium flow (50 $cm^3\,min^{-1}$) and then cooled to the specified reaction temperature. Laboratory scale activity tests were carried out in an integral monolith reactor, operating under atmospheric pressure at temperature of 673 K and at various space times. Space times were changed by varying the monolith volume (or monolith length) at constant total flow rate of the reactant gas (10 $cm^3\,min^{-1}$). The temperature of the reactant gas (4% NO/He); Messer Griesheim) was monitored by the thermocouple (Ni–CrNi) placed at the exit of the monolith. The catalyst activity for NO removal was evaluated by conversion of NO into N_2 when the reaction reached steady-state (30 min from the exposure to stream). The reaction products were analysed by GC (Varian 3300) using molecular sieve 5A, thermal conductivity detector and helium as the carrier gas. The details about the experimental apparatus and procedures for the reaction product analysis are given elsewhere [8].

3. Description of mathematical models

3.1. Assumptions

In this work specific aspects associated with mathematical modelling of the experimental monolith reactor were addressed. Two heterogeneous models, accounting for a 1D description of gas phase and 2D description of solid phase (model I) and for 2D description of both gas and solid phase (model II) were applied for simulation of the monolith reactor. Main assumptions used to develop the models were: steady-state conditions, equal conditions within each monolith channel (single channel analysis), plug flow and negligible pressure drop along the monolith channel (ca. 50 Pa). Due to the low concentration of the reactant and a small amount of heat generated by the reaction, the reaction was considered isothermal. Axial diffusion in the gas and solid phase was neglected. The problem of changed geometry of the channels after washcoating was simplified applying the "equivalent ring-zone approximation" [12]. The equivalent thickness of the catalytic layer was 0.217 and 0.527 mm for the monoliths MZ1 and MZ2, respectively.

3.2. Governing equations

3.2.1. Model I

Model I was represented by the following partial differential equations (PDEs):

(a) for the reactant concentration in the fluid phase ($0 < r < r_{ch}$)

$$u\frac{\partial C_{A,f}}{\partial z} = k_m a(C_{A,f} - C_{A,s}) \quad (1)$$

(b) for the reactant concentration in the solid phase ($r_{ch} < r < R$)

$$D_e\left(\frac{\partial^2 C_{A,s}}{\partial r^2} + \frac{1}{r}\frac{\partial C_{A,s}}{\partial r}\right) - r_{A,s} = 0 \quad (2)$$

The boundary conditions were defined as follows:

$$C_{A,s} = C_{A,f} = C_{A_0}, \quad \text{at } z = 0 \quad (3)$$

$$D_e\frac{\partial C_{A,s}}{\partial r} = -k_m(C_{A,f} - C_{A,s}), \quad \text{at } r = r_{ch} \quad (4)$$

$$\frac{\partial C_{A,s}}{\partial r} = 0, \quad \text{at } r = R(R = r_{ch} + \delta_e) \quad (5)$$

As shown, the model I was based on the assumption of the constant concentration in the fluid phase and on the simultaneous intraphase diffusion and chemical reaction in the solid phase (i.e. catalytic layer).

3.2.2. Model II

Model II was used to provide a complete 2D description of both fluid and solid phase (i.e. axial and radial dependent concentration in both phases). The resulting equations were

(a) for the reactant concentration in the fluid phase ($0 < r < r_{ch}$)

$$u\frac{\partial C_{A,f}}{\partial z} - D_f\left(\frac{\partial^2 C_{A,f}}{\partial r^2} + \frac{1}{r}\frac{\partial C_{A,f}}{\partial r}\right) = 0 \quad (6)$$

(b) for the reactant concentration in the solid phase ($r_{ch} < r < R$)

$$D_e\left(\frac{\partial^2 C_{A,s}}{\partial r^2} + \frac{1}{r}\frac{\partial C_{A,s}}{\partial r}\right) - r_{A,s} = 0 \quad (7)$$

The appropriate boundary conditions were

$$C_{A,s} = C_{A,f} = C_{A_0}, \quad \text{at } z = 0 \quad (8)$$

$$\frac{\partial C_{A,f}}{\partial r} = 0, \quad \text{at } r = 0 \quad (9)$$

$$D_f\frac{\partial C_{A,f}}{\partial r} = D_e\frac{\partial C_{A,s}}{\partial r}, \quad \text{at } r = r_{ch} \quad (10)$$

$$\frac{\partial C_{A,s}}{\partial r} = 0, \quad \text{at } r = R \quad (11)$$

$$\frac{\partial C_{A,s}}{\partial z} = 0, \quad \text{at } z = Z \quad (12)$$

3.3. Reaction rate

Many studies have been carried out to identify the nature of the active sites [13–16] and the mechanism of the NO decomposition [17–20]. However, only a few measurements of kinetic parameters have been reported [21–24]. Kinetic study of NO decomposition over Cu/ZSM-5 zeolite has been described in detail in our previous papers and some of the kinetic data presented in this paper were contained in those studies [24,25]. Briefly, experimental kinetic data obtained using powder Cu/ZSM-5 catalyst were correlated with several mechanistic kinetic models. The best agreement between experimental data and theoretical prediction was achieved by the following rate equation:

$$r_{A,s} = \frac{kC_{A,s}^2}{(1 + \sqrt{K'_D C_{O_2}})^2} \quad (13)$$

The mechanistic kinetic model (Eq. (13)) was derived by defining surface reaction between two adsorbed NO molecules as the rate-determining step (RDS), as shown below:

$$NO + * \underset{k_{-A}}{\overset{k_A}{\rightleftarrows}} NO^*, \qquad K_A = \frac{k_A}{k_{-A}} \quad (14)$$

$$2NO^* \xrightarrow{k_S} N_2 + 2O^* \quad \text{(RDS)} \quad (15)$$

$$2O^* \underset{k_{-D}}{\overset{k_D}{\rightleftarrows}} O_2 + 2^* \quad \left(K'_D = \frac{k_{-D}}{k_D}\right) \quad (16)$$

In the proposed reaction mechanism (Eqs. (14)–(16)), term * represents an empty active site on the surface of the catalyst, while NO* and O* are adsorbed NO and O, respectively. A site balance for the total concentration of sites, C_t (Eq. (17)),

$$C_t = C_* + C_{NO^*} + C_{O^*} = C_*(1 + K_A C_{A,s} + \sqrt{K'_D C_{O_2}}) \quad (17)$$

combined with quasiequilibrated steps [14,16], gives the rate equation [18]:

$$r_{A,s} = k_S C_{NO^*}^2 = \frac{k_S(K_A C_t C_{A,s})^2}{(1 + K_A C_{A,s} + \sqrt{K'_D C_{O_2}})^2} \quad (18)$$

If the term representing the adsorbed NO is assumed small compared with other terms in the denominator (e.g. $K_A C_{A,s} \ll 1 + \sqrt{K'_D C_{O_2}}$), then Eq. (18) can be reduced to the form of Eq. (13). Proposed reaction mechanism is consistent with the observed redox behaviour of copper ions in the ZSM-5 zeolite [15,17]. The same reaction mechanism is proposed by Vannice et. al. [20] to describe the rate of NO reduction by CH_4 as well NO decomposition over La_2O_3 and Sr/La_2O_3 catalysts.

3.4. Numerical methods

The above governing equations constituted a boundary value problem involving a set of the coupled partial differential equations. They were resolved using the method of lines. The mass transfer coefficient (k_m) and the rate constant value (k) were regarded as the adjustable parameters of the reactor model I, while the effective diffusion coefficient (D_e) and the rate constant (k) were regarded as the adjustable parameters of the reactor model II. Preliminary modelling study was performed using adsorption equilibrium constant (K'_D) as the adjustable parameter in the both models too. The estimated value of K'_D was found to be $0.02\,m^3\,mol^{-1}$. This value was in qualitative agreement with that reported by Li and Hall [21]. However, the results of parametric sensitivity revealed that the value of K'_D has small influence on the results of simulation. Therefore all subsequent computations were performed only with two adjustable parameters in order to avoid uncertainty due to great number of parameters (using K'_D as constant value).

The parameters of the reactor models were assessed using a modified differential method of data analysis and Nelder–Mead method of non-linear optimisation [26]. The initial values used for estimation were previously reported values of the kinetic parameters for Cu/ZSM-5 catalyst powder, ground to very fine particles so as to avoid the internal diffusion limitation [24]. Correlation criterion was a mean square deviation between the experimentally obtained and theoretically predicted values, S.D. Due to the radial concentration gradients in the fluid phase (model II), average values across the reactor channel were computed to compare simulation with the experimental values (Eq. (19)).

$$\overline{C_{A,f}}(z) = \frac{\int_0^{r_{ch}} u(r) C_{A,f}(z,r) 2\pi\,dr}{\int_0^{r_{ch}} u(r) 2\pi\,dr}, \quad \text{at } z = Z \tag{19}$$

The Chapman–Enskog formula was used to calculate the molecular diffusion coefficient (D_f) [27]. The estimated value of the effective diffusion coefficient (D_e) from the reactor model II was applied as constant value in the reactor model I. Similar value was obtained using the parallel pore model, as described in [9].

4. Results and discussion

4.1. Simulation of the experimental data

The modelling and simulation of a monolith reactor can be performed using mathematical models of varying complexity. However, models are only as good as the way in which the physico-chemical processes are modelled and the quality of the physical and chemical parameters (e.g. kinetic expressions, physical properties, etc.) acquired for use in the models [28].

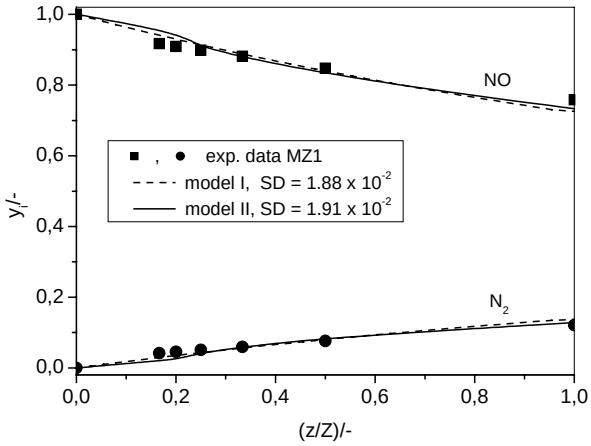

Fig. 1. Comparison between experimental data (points) and the values predicted by the models (lines) for the monolith sample MZ1.

This paper compares theoretical predictions obtained with two different heterogeneous models of the monolith reactor (model I, Eqs. (1)–(5) and model II, Eqs. (6)–(12)) and analyses their range of acceptability. Simulation results for both models are shown in Fig. 1. There is apparently a good agreement between the experimental data and theoretical predictions obtained for both models. This arises from the fact that both models use two adjustable parameters. From the modelling perspective, both models are acceptable, especially nowadays when the computers are rapidly getting faster. Main features of both models will be pointed out later in this paper.

The comparison between the experimental data and the values predicted for the monolith samples MZ1 ($\delta_e = 0.217$ mm) and MZ2 ($\delta_e = 0.527$ mm) by model II is illustrated in Fig. 2. As expected, the molar fraction of unreacted NO at the reactor exit decreases with the increased thickness of the catalytic layer due to higher number of the active sites, indicating simultaneously good porosity of the catalytic layer. Estimated values of the reaction rate con-

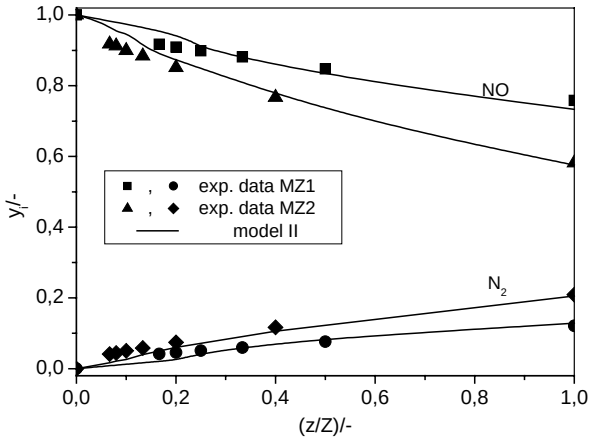

Fig. 2. Comparison between experimental data (points) and the values predicted by the model II (lines) for the monolith samples MZ1 ($\delta_e = 0.217$ mm) and MZ2 ($\delta_e = 0.527$ mm).

Table 1
Estimated values of the reaction rate constant, k, for powder Cu/ZSM-5 catalyst and monoliths (MZ1 and MZ2) at 673 K

Catalyst sample	k ($\times 10^{-2}$ m^3 mol^{-1} s^{-1})
Powder Cu/ZSM-5	9.4
Monolith MZ1	1.0
Monolith MZ2	3.6

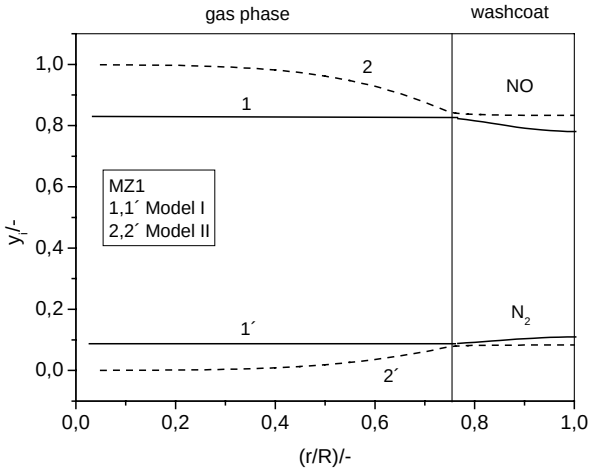

Fig. 3. Radial profiles of the molar fractions of NO and N_2 for the monolith MZ1 at 25% of the monolith reactor length.

stant, k, for the monolith samples MZ1 and MZ2 at 673 K, predicted by model II are given in Table 1. For comparison purposes, there are also values of rate constant for the powder Cu/ZSM-5 catalyst. Some difference in the rate constant for the powder zeolite catalyst and monoliths containing zeolite washcoat are recorded. As mentioned in the experimental part, aluminium nitrate is used as the binder during the preparation of the monolith catalyst. This could result in the changed structure of the catalytic washcoat (the change in the physical properties, the change of the active sites structure, etc.) compared to powder Cu/ZSM-5 catalyst.

Fig. 3 illustrates the radial molar fraction profiles of NO and N_2 in the fluid and solid phase (washcoat) for the monolith MZ1 at 25% of the monolith reactor length obtained using models I and II. Based on the main assumptions made during development of the models, the flat radial profiles in the fluid phase and theoretical curves, corresponding to the radial diffusion in the fluid phase, are obtained using model I and II, respectively. Similar results are obtained for the monolith MZ2 (Fig. 4).

4.2. Fluid–solid interphase mass transfer

The important feature of the multi-dimensional models is that they enable calculation of the local Sherwood (Sh) numbers and corresponding mass transfer coefficients along the length of the monolith channel under reaction conditions [7,29].

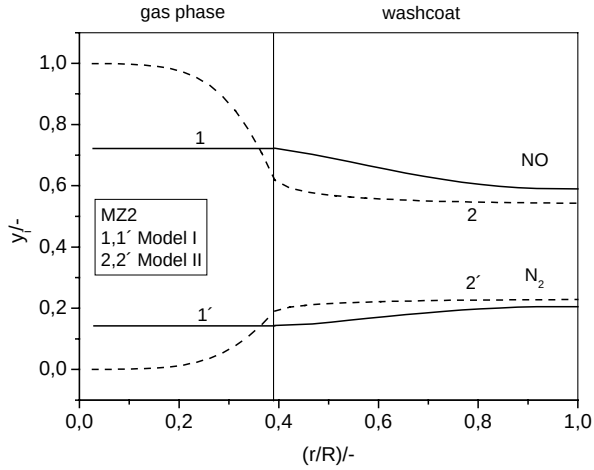

Fig. 4. Radial profiles of the molar fractions of NO and N_2 for the monolith MZ2 at 25% of the monolith reactor length.

The local mass transfer coefficients and corresponding Sh numbers can be calculated from the boundary condition given by Eq. (4), i.e. applying Eqs. (20) and (21):

$$k_m(z) = \frac{D_e(\partial C_{A,s}/\partial r)}{C_{A,s} - C_{A,f}} \quad (20)$$

$$Sh(z) = \frac{k_m(z) d_{ch}}{D_f} \quad (21)$$

This approach is based on the boundary layer theory, meaning that the mass transfer resistance is concentrated on a very thin and stagnant film near the walls of the monolith channel [30]. Apparently, concentration in the fluid phase ($C_{A,f}$) is a constant value, which is based on the assumption made during development of the model I.

Applying the complete 2D model (model II), the local Sh numbers and corresponding mass transfer coefficients can be formally calculated in the similar way, taking into account the boundary condition given by Eq. (10), i.e. applying Eqs. (21) and (22):

$$k_m(z) = \frac{D_f(\partial C_{A,f}/\partial r)}{C_{A,s} - \bar{C}_{A,f}} \quad (22)$$

Due to the existence of the radial concentration profile across the monolith channel, the new term, $\bar{C}_{A,f}$ appears in Eq. (22), which represents mean concentration in the fluid phase and can be calculated using Eq. (19). It is important to note that under the condition given by Eqs. (6)–(12) (i.e. by the model II) the whole radius of the monolith channel is regarded as the boundary layer in the moving fluid. Calculation of the local Sh and mass transfer coefficients using the above described approach is common to many researchers [7,29,31–33].

It is interesting to compare the values of the local Sh numbers and mass transfer coefficients obtained from Eqs. (20) and (21) (model I), and Eqs. (21) and (22) (model II). This comparison for the monolith MZ1 is displayed in Fig. 5. As shown, the mass transfer coefficients and especially the

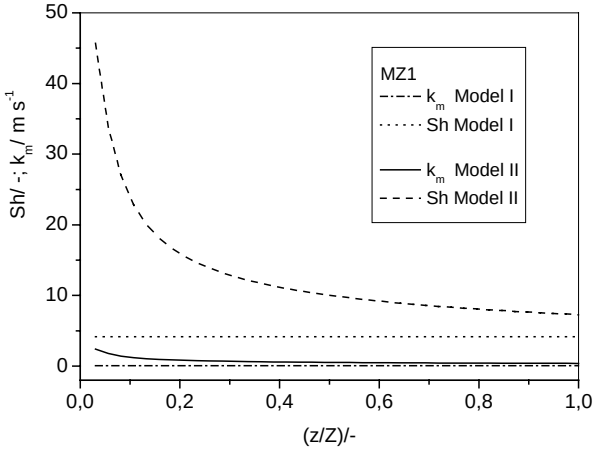

Fig. 5. Local *Sh* numbers and mass transfer coefficients predicted by the model I and model II as the function of normalised channel length for the monolith MZ1.

Sh numbers predicted by the model II are very high at the entry of the monolith reactor, and their values decrease downstream the reactor. Similar results are obtained for the monolith MZ2, as shown in Fig. 6. On the other hand, the appropriate values obtained applying the model I are smaller and almost unchanged in the axial direction. It is evident that the prediction of the local mass transfer coefficient and corresponding *Sh* numbers is not a simple task. High values of k_m and *Sh* at the entry of the reactor can be explained taking into account concentration difference (denominator in Eq. (22)) being very small in the entry region of the reactor. However, along the monolith length the concentration differences increase because mean concentration of the relevant variable in the fluid phase ($\bar{C}_{A,f}$) decreases. This is supported by the results displayed in Figs. 7 and 8, where the radial profiles of NO and N_2 predicted by models I and II are shown at different positions along the monolith length. Mean concentration in the fluid phase decreases along the

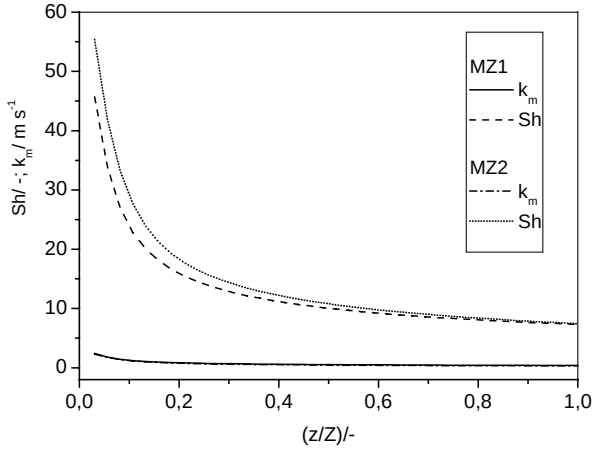

Fig. 6. Local *Sh* numbers and mass transfer coefficients predicted by the model II as the function of normalised channel length for the monoliths MZ1 and MZ2.

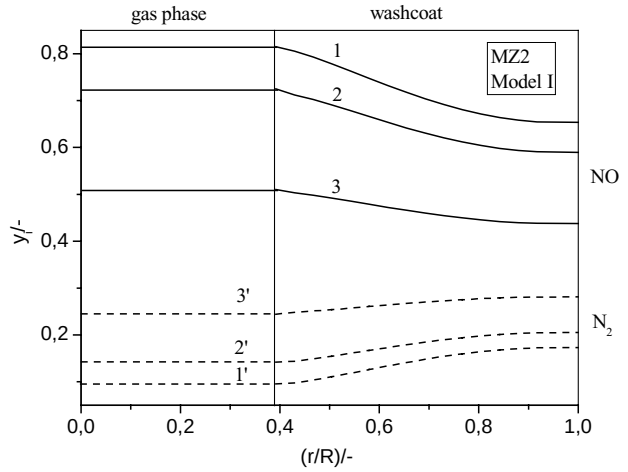

Fig. 7. Radial profiles of the molar fractions of NO (solid) and N_2 (dash) predicted by the model I for the monolith MZ2 at different positions along the monolith length. 1,1′—at 5%; 2,2′—at the 25%; 3,3′—at the exit from the reactor.

monolith length not only due to the chemical reaction in the catalytic layer, but also due to the developing radial diffusion profile in the fluid phase (the process of molecular diffusion). It is important to emphasise that mean concentration in the fluid phase is always higher then the "true" concentration which is the nearest to the surface of the catalytic layer (at the wall surface on the fluid-phase side). On the other hand, if the concentration in the first point near to the surface of the catalyst layer (extracted from the numerical procedure) is applied in the Eq. (22) instead of $\bar{C}_{A,f}$, the overall difference between the calculated values of the k_m and *Sh* numbers at the entry region of the reactor and corresponding values at the exit from the reactor becomes smaller. The results of such calculations are illustrated in Fig. 9 (dash line).

Obviously, calculation of the local *Sh* numbers and mass transfer coefficients across the boundary layer in the moving

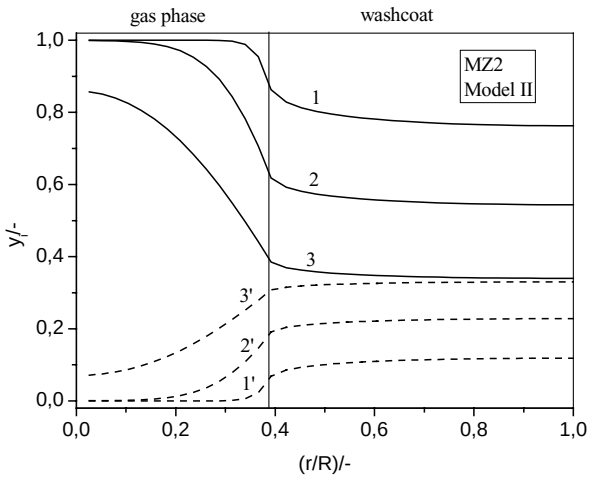

Fig. 8. Radial profiles of the molar fractions of NO (solid) and N_2 (dash) predicted by the model II for the monolith MZ2 at different positions along the monolith length. 1,1′—at 5%; 2,2′—at the 25%; 3,3′—at the exit from the reactor.

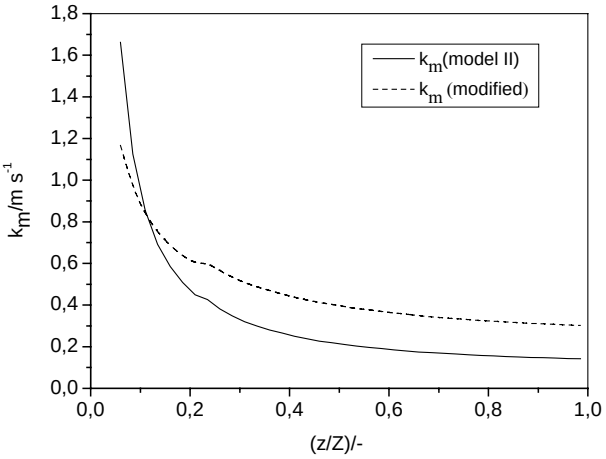

Fig. 9. Local mass transfer coefficients predicted for the monolith MZ2 predicted by the model II (solid line) and modified (dash line).

fluid by using the analogy with the boundary layer theory (i.e. by using Eq. (22)) may lead to the values which are overestimated and questionable.

5. Conclusions and outlook

The agreement between the calculated and experimental results supports the overall ability of the proposed models to account for the influence of both inter- and intraphase mass transfer on the performance of the monolith reactor.

Generally, a good agreement between the experimental data and theoretical predictions was obtained for both models due to the adjustable parameters. Different values, obtained with the two applied models, for the interphase mass transfer coefficients and the corresponding *Sh* numbers (Figs. 7 and 8) could be attributed to different assumptions made during development of the models. Due to a detailed consideration of the physico-chemical processes occurring in the catalytic monolith, the both models provided valuable insight into the performance of the monolith reactor.

In the future work particular emphasis will be put on independent experimental measurement of the parameters of the monolith reactor model, such as the effective diffusion coefficient in the catalytic layer, providing suitability of the reactor models considered in this paper.

Acknowledgements

The authors highly acknowledge financial support of the Croatian Ministry of Science and Technology. Special thanks go to R.M. Heck of Engelhard Corporation for providing cordierite honeycombs and to Degussa for supplying the authors with ZSM-5 zeolite.

References

[1] S. Irandoust, A. Cybulski, J.A. Moulijn, The use of monolithic catalysts for three-phase reactions, in: A. Cybulski, J.A. Moulijn (Eds.), Structured catalysts and reactors, Marcel Dekker, New York, 1998, pp. 239–265.
[2] T.A. Nijhuis, F. Kapteijn, J.A. Moulijn, Monolithic catalysts as more efficient reactors in three-phase applications, in: A. Corma, F.V. Melo, S. Mendioroz, J.L.G. Fierro (Eds.), Studies in Surface Science Catalysis, vol. 130, Elsevier, Amsterdam, 2000, pp. 2735–2740.
[3] P. Canu, Catal. Today 64 (2001) 239.
[4] R.M. Heck, S. Gulati, R.J. Farrauto, Chem. Eng. J. 82 (2001) 149.
[5] F. Kapteijn, T.A. Nijhuis, J.J. Heiszwolf, J.A. Moulijn, Catal. Today 66 (2001) 133.
[6] M.F.M. Zwinkels, S.G. Järås, P.G. Menon, T.A. Griffin, Catal. Rev.-Sci. Eng. 35 (1993) 319.
[7] G. Groppi, E. Tronconi, Chem. Eng. Sci. 52 (29) (1997) 3521.
[8] V. Tomašić, Z. Gomzi, S. Zrnčević, React. Kinet. Catal. Lett. 77 (2) (2002) 245.
[9] V. Tomašić, Z. Gomzi, Chem. Eng. Proc. 43 (2004) 765.
[10] X. Xu, J.A. Moulijn, in: A. Cybulski, J.A. Moulijn (Eds.), Structured Catalysts and Reactors, Marcel Dekker, New York, 1998, pp. 599–617.
[11] T.A. Nijhuis, A.E.W. Beers, T. Vergunst, i. Hoek, F. Kapteijn, J.A. Moulijn, Catal. Rev. 43 (4) (2001) 345–380.
[12] H.P. Calis, K. Takács, A.W. Gerritsen, C.M. van den Bleek, Bead-String reactor, in: A. Cybulski, J.A. Moulijn (Eds.), Structured Catalysts and Reactors, Marcel Dekker, New York, 1998, pp. 355–392.
[13] V.I. Parvulescu, M.A. Centeno, P. Grange, B. Delmon, J. Catal. 191 (2000) 445.
[14] Y. Zhang, M. Flytzani-Stephanopoulos, J. Catal. 164 (1996) 131.
[15] M. Iwamoto, H. Yahiro, N. Mizuno, W.X. Zhang, Y. Mine, H. Furukawa, S. Kagawa, J. Phys. Chem. 96 (1992) 9360.
[16] B. Wichterlová, J. Dědeček, A. Vondrová, J. Phys. Chem. 99 (4) (1995) 1065.
[17] M. Iwamoto, H. Yahiro, Catal. Today 22 (1994) 5.
[18] M. Shelef, Catal. Lett. 15 (1992) 305.
[19] A.W. Aylor, S.C. Larsen, J.A. Reimer, A.T. Bell, J. Catal. 157 (1995) 592.
[20] M.A. Vannice, A.B. Walters, X. Zhang, J. Catal. 159 (1996) 119.
[21] Y. Li, W.K. Hall, J. Catal. 129 (1991) 202.
[22] Y. Li, J.N. Armor, Appl. Catal. B: Environ. 2 (1993) 239.
[23] Y. Li, J.N. Armor, J. Catal. 150 (1994) 376.
[24] V. Tomašić, Z. Gomzi, S. Zrnčević, Appl. Catal. B: Environ. 18 (1998) 233.
[25] V. Tomašić, Z. Gomzi, S. Zrnčević, React. Kinet. Catal. Lett. 64 (1998) 89.
[26] J.H. Mathew, Numerical Methods for Computer Science, Engineering and Mathematics, Prentice-Hall, Fullerton, 1987, 295 pp.
[27] J.M. Smith, Chemical Engineering Kinetics, McGraw-Hill, New York, 1981, 450 pp.
[28] S.T. Kolaczkowski, Catal. Today 47 (1999) 209.
[29] R.E. Hayes, S.T. Kolaczkowski, Catal. Today 47 (1999) 295.
[30] W.G. Whitman, Chem. Met. Eng. 29 (1923) 146.
[31] R.E. Hayes, S.T. Kolaczkowski, Chem. Eng. Sci. 49 (21) (1994) 3587.
[32] B. Roduit, A. Baiker, F. Bettoni, J. Baldyga, A. Wokaun, AIChE J. 44 (12) (1998) 2731.
[33] R. Wanker, H. Raupenstrauch, G. Staudinger, Chem. Eng. Sci. 55 (2000) 4709.